ChemComm

COMMUNICATION

View Article Online
View Journal | View Issue

Cite this: *Chem. Commun.*, 2023, 59, 8532

Received 6th May 2023,
Accepted 8th June 2023

DOI: 10.1039/d3cc02216a

rsc.li/chemcomm

Infrared spectroscopic and theoretical investigations of novel iridium oxyfluorides†

Yan Lu, Robert Medel, Guohai Deng and Sebastian Riedel *

The iridium oxyfluorides (OIrF, $OIrF_2$ and FOIrF) were prepared for the first time by the reaction of IR-laser ablated iridium atoms and OF_2, isolated in solid neon and argon matrices. The assignments of the main vibrational absorptions of these products were supported by a combined analysis of IR-matrix-isolation spectroscopy with $^{18}OF_2$ substitution and quantum-chemical calculations. The OIrF molecule exhibits triple bond character. In contrast to terminal oxyl radical species $OPtF_2$ and $OAuF_2$, a much lower spin-density contribution at the oxygen atom was found in $OIrF_2$.

Iridium, one of the rarest transition metal elements in the earth's crust, is the only confirmed chemical element capable of attaining the highest oxidation state +IX in the iridium tetroxide cation $[IrO_4]^+$.[1] In general, apart from oxides, the family of such compounds with transition metals in their highest oxidation states includes fluoride and oxyfluoride molecules.[1,2] The +I to +VI oxidation states of Ir have been experimentally observed in binary iridium fluorides, with most studies focusing on the characterization of the IrF_6 molecule.[3–6] However, less is known about iridium oxyfluorides from both theoretical and experimental perspectives.[5–10] The $IrOF_5$ molecule was predicted by us as an alternative target for oxidation state +VII.[7] To the best of our knowledge, iridium oxyfluorides have not yet been experimentally verified, although various methods and approaches have been proposed to produce them over the years, typically based on hexafluorides as reactants.[5,6,8–10]

The generation of iridium oxyfluorides was first proposed by Ruff and Fischer in 1929 in the reaction of iridium hexafluoride with the alkali present in the glass.[5] However, the produced iridium oxyfluoride in this reaction was later identified to the complex salts of quinquevalent iridium in 1956.[6,9] In the following decades, some other methods were also tried out to prepare iridium oxyfluorides, such as fluorination of iridium dioxide,[6] oxygen–fluorine exchange[10] and hydrolysis reactions.[8] Unfortunately, there were no iridium oxyfluorides observed, which were proposed to be extremely unstable intermediate products, while the methods have been used successfully in the preparation of other transition metal oxyfluorides ($ReOF_4$, $OsOF_4$, UOF_4, *etc.*).[8,10] Therefore, due to their highly reactive nature, it is still a challenge to develop a useful procedure to prepare the so far experimentally unknown class of iridium oxyfluorides.

An established quite efficient and facile route to produce oxyfluoride molecules under cryogenic conditions in rare gas matrices is the reaction of laser-ablated metal atoms with OF_2.[11–17] The successful preparation and identification of such compounds indicate that synthesizing iridium oxyfluorides might be possible as well. In this work, we describe for the first-time the preparation of molecular iridium oxyfluorides (OIrF, $OIrF_2$ and FOIrF) *via* the reaction of laser-ablated iridium atoms with OF_2 in excess neon and argon at cryogenic temperatures. The matrix-isolation infrared spectroscopic identification of these new oxyfluorides is supported by isotope labelling of $^{18}OF_2$ and quantum-chemical calculations.

The infrared spectra from the reactions of laser-ablated iridium atoms with either $^{16}OF_2$ or $^{18}OF_2$ in solid neon (5 K) followed by annealing and irradiation are shown in Fig. 1. The spectra from analogous experiments in solid argon (12 K) are shown in Fig. S1 in the ESI.† The observed and calculated vibrational frequencies are summarized in Table 1 and Tables S1–S6 (ESI†).

The diatomic OF radical is the most common species in the spectra from the reactions of OF_2 and laser-ablated metal atoms and its absorption was observed at 1031.3/1028.6 cm^{-1} (^{16}OF in solid Ne/Ar) and at 1000.2/997.7 cm^{-1} (^{18}OF in solid Ne/Ar).[12,18] The bands at 643.6 and 697.8 cm^{-1} were obtained in the reaction of Ir with F_2 in excess neon, which have previously been assigned to IrF and IrF_5, respectively.[3] In addition to these known fluoride molecules, in the present work, newly formed product absorptions were observed clearly at 666.8, 672.6, 685.1, 889.3 and 984.1 cm^{-1} (Fig. 1(a)). The less intense absorption 685.1 cm^{-1} and a weak absorption at 889.3 cm^{-1}

Freie Universität Berlin, Department for Chemistry and Biochemistry, Fabeckstr. 34/36, Berlin, Germany. E-mail: s.riedel@fu-berlin.de

† Electronic supplementary information (ESI) available. See DOI: https://doi.org/10.1039/d3cc02216a

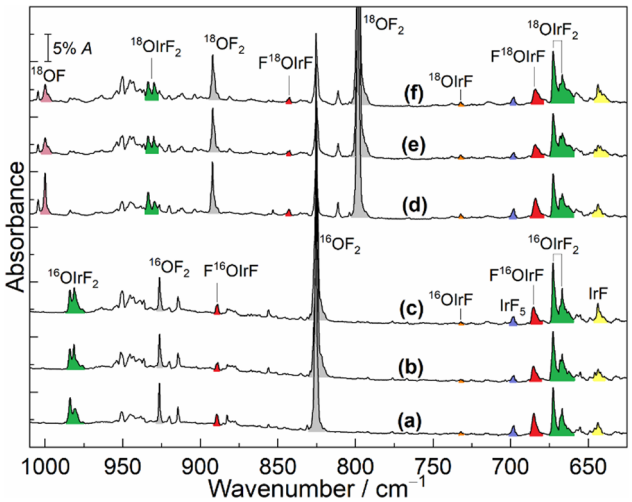

Fig. 1 IR spectra in the neon matrix at 5 K. (a) IR spectrum of the reaction products of laser-ablated Ir atoms with 0.02% $^{16}OF_2$; (b) after annealing to 9 K; (c) after full arc (>220 nm) irradiation for 15 min; (d) IR spectrum of reaction products of laser-ablated Ir atoms with 0.1% $^{18}OF_2$; (e) after annealing to 9 K; (f) after full arc (>220 nm) irradiation for 15 min.

decreased substantially after annealing to 9 K, but both absorptions increased slightly when the sample was further exposed to $\lambda > 220$ nm irradiation. However, both sample annealing and irradiation resulted in an increase of the above mentioned bands at 666.8, 672.6 and 984.1 cm^{-1}. The spectra were also recorded after sample deposition in solid argon (Fig. S1, ESI†). Apart from the known species IrF, IrF_2 and IrF_4,[3] the newly observed bands at 657.5, 663.6 and 976.0 cm^{-1} in solid argon on deposition show continued growth during annealing and irradiation of the sample.

To aid in the assignment of the new bands, all the experiments in neon and argon matrices were repeated by employing the isotopically enriched reagent $^{18}OF_2$ under similar conditions (Fig. 1 and Fig. S1, ESI†). According to the almost same behaviour of the absorptions during annealing and subsequent broadband irradiation, a large red-shift of 46.4 cm^{-1} was observed for the 889.3 cm^{-1} band in the neon matrix, while the more intense band 685.1 cm^{-1} displayed a small $^{16/18}$O-isotopic shift of 1.0 cm^{-1}. Moreover, the band at 984.1 cm^{-1} showed a distinct red-shift of 50.4 cm^{-1}, whereas no shifts were observed for the two strong bands at 666.8 and 672.6 cm^{-1} upon ^{18}O substitution. In the argon matrix, there were almost no $^{16/18}$O shifts for bands at 657.5 and 663.6 cm^{-1}. However, the higher wavenumber signal at 976.0 cm^{-1} displayed a noticeable isotopic shift of 50.2 cm^{-1}.

The bands at 666.8, 672.6 and 984.1 cm^{-1} in the neon matrix (657.5, 663.6 and 976.0 cm^{-1}, Ar-matrix) produced in the Ir and OF_2 reactions were not observed when Ir was reacted with F_2 or O_2 in previous matrix-isolation investigations.[3,19,20] This group of bands should be due to the different vibrational modes of iridium oxyfluoride molecules based on their identical behaviours throughout the experiments. Since the bands at 666.8 and 672.6 cm^{-1} in the neon matrix (657.5 and 663.6 cm^{-1}, Ar-matrix) are located in the region of Ir–F stretching mode absorptions and show almost no $^{16/18}$O-isotopic shifts, they are assigned to the symmetric and antisymmetric F–Ir–F stretches of this new molecule, respectively. The higher wavenumber band at 984.1 cm^{-1} is shifted to 933.7 cm^{-1} with an $^{16}O/^{18}O$ frequency ratio of 1.0540, which is close to the value of diatomic IrO (1.0530),[19] indicating a terminal Ir–O stretch. Hence, based on the observation of two F–Ir–F stretches and one terminal Ir–O, the new molecule is identified as $OIrF_2$.

The assignment of $OIrF_2$ is also further supported by quantum-chemical calculations. The $OIrF_2$ molecule is predicted to have three infrared-active absorptions above 600 cm^{-1} at CCSD(T) and B3LYP levels (Table 1 and Tables S1, S2, ESI†). The observed band positions at 666.8 and 672.6 cm^{-1} in the neon matrix (657.5 and 663.6 cm^{-1}, Ar-matrix) are consistent with the calculated symmetric and antisymmetric F–Ir–F stretches at 682.8 and 684.1 cm^{-1} and no $^{16/18}$O shifts were observed at the CCSD(T) level (670.5 and 671.7 cm^{-1}, B3LYP level). Similar to most of the other metal oxydifluorides OMF_2,[11,12,15–17] the predicted harmonic vibrational wavenumbers of M–O are larger than the experimental fundamentals due to neglected anharmonicity.[17] However, the calculated $^{16/18}$O-isotopic shifts due to Ir–O stretching at the CCSD(T) ($\Delta\nu(^{16/18}O)$ = 54.5 cm^{-1}) and B3LYP levels ($\Delta\nu(^{16/18}O)$ = 55.2 cm^{-1}) are in good agreement with the observed ones of ($\Delta\nu(^{16/18}O)$ = 50.4 cm^{-1}) Ne-matrix and ($\Delta\nu(^{16/18}O)$ = 50.2 cm^{-1}) Ar-matrix, further supporting the assignments for $OIrF_2$.

The set of absorptions at 685.1 and 889.3 cm^{-1} in the spectra belongs to another new product molecule. Both bands

Table 1 Calculated and experimentally observed IR wavenumbers (in cm^{-1}) of iridium oxyfluorides[a]

	Exp.						Calc.			
	Ne			Ar			CCSD(T)[b]			
Species	$\nu(^{16}O)$	$\nu(^{18}O)$	$\Delta\nu$	$\nu(^{16}O)$	$\nu(^{18}O)$	$\Delta\nu$	$\nu(^{16}O)$	$\nu(^{18}O)$	$\Delta\nu$	Modes
OIrF	—[c]	—[c]	—[c]	—[c]	—[c]	—[c]	1053.4	998.0	55.4	ν(Ir–O)
($^1\Sigma^+$, $C_{\infty v}$)	732.2	732.2	0.0	—[c]	—[c]	—[c]	741.7	741.4	0.3	ν(Ir–F)
$OIrF_2$	984.1/980.7	933.7/929.6	50.4/51.1	976.0/973.6	925.8/922.6	50.2/51.0	1033.1	978.6	54.5	ν(Ir–O)
($^2B_1$, C_{2v})	672.6	672.6	0.0	663.6	663.6	0.0	684.1	684.1	0.0	$\nu_{as}(IrF_2)$
	666.8	666.8	0.0	657.5	657.5	0.0	682.8	682.8	0.0	$\nu_s(IrF_2)$
FOIrF	889.3	842.9	46.4	—[c]	—[c]	—[c]	938.5	890.6	47.9	ν(Ir–O)
($^2A''$, C_s)	685.1	684.1	1.0	—[c]	—[c]	—[c]	698.1	697.9	0.2	ν(Ir–F)
	—[c]	—[c]	—[c]	—[c]	—[c]	—[c]	464.4	446.1	18.3	ν(O–F)

[a] The complete set of calculated frequencies is provided in the ESI (Tables S1–S6). For the CCSD(T) calculations no intensities are available. [b] Harmonic frequencies calculated at the CCSD(T)/aug-cc-pVTZ-PP level. [c] Bands were not observed, or too weak.

were detected in the neon matrix after sample deposition and decreased dramatically on sample annealing, which can be assigned to the molecule FOIrF. Surprisingly, the corresponding bands of this product were not detected in solid argon. Similar to the small $^{16/18}$O-isotope shift of 3.3 cm^{-1} of the Pd–F stretching in molecule FOPdF,[12] the band at 685.1 cm^{-1} exhibits a small but significant $^{16/18}$O-isotopic shift of 1.0 cm^{-1} and is associated with the Ir–F stretching band of this hypofluorite. Both the band positions and $^{16/18}$O-isotopic shifts show good agreement with the predicted wavenumbers at 698.1 cm^{-1} and the $^{16/18}$O-isotope shift of 0.2 cm^{-1} at the CCSD(T) level (Table 1 and Table S4, ESI†). Moreover, while the calculated wavenumber (938.5 cm^{-1}) for Ir–O stretching in FIrOF is higher than the experimental value (889.3 cm^{-1}), the predicted $^{16/18}$O shift of 47.9 cm^{-1} is in good agreement with the experimental value (46.4 cm^{-1}), similar to $OIrF_2$. The ^{16}O–F and ^{18}O–F vibrational stretches in FIr$^{16/18}$OF are computed at 464.4 and 446.1 cm^{-1} at the CCSD(T) level, respectively, but our search for both bands was unsuccessful in the detection range of our FTIR spectrometer (MCT-B detector, 4000–450 cm^{-1}).

Since OMF was the major product from the reaction of hot metal atoms with OF_2,[11–17] the formation of the elusive OIrF in the experiments should also be considered. In contrast to the very strongly IR-active Au–F stretch and the extremely weakly IR-active Au–O stretch in OAuF,[11] the B3LYP calculation predicts two absorbances for OIrF at 735.4 and 1106.0 cm^{-1} with an approximate intensity ratio of 4 : 3 (Table 1 and Tables S5, S6, ESI†). The Ir–F band in OIrF is tentatively assigned to a weak band at 732.2 cm^{-1} with almost no $^{16/18}$O-isotopic shift in solid neon, which has a large blue-shift of 88.6 cm^{-1} relative to the stretching vibration in IrF (643.6 cm^{-1}, Ne-matrix).[3] However, the O–Ir fundamental of this species was expected to be located at 1106.0 ($\Delta\nu(^{16/18}O)$ = 58.5 cm^{-1}) or 1053.4 cm^{-1} ($\Delta\nu(^{16/18}O)$ = 55.4 cm^{-1}) from B3LYP and CCSD(T) calculations, respectively. It is reasonable that this mode was not observed in this work because it is even weaker than the 732.2 cm^{-1} band. Similar to the cases of OPtF and OAuF,[11,12] attempts to detect the species OIrF in argon matrices failed, which is most likely due to the stronger Ar interactions with the formed intermediate species. In argon experiments, only the $OIrF_2$ product was produced and identified by IR spectroscopy (Fig. S1, ESI†).

To get further insights into the structures and electronic configurations of the new species, the iridium oxyfluorides OIrF, FOIrF and $OIrF_2$ were calculated at the DFT and CCSD(T) levels in conjunction with scalar relativistic pseudopotentials. All possible spin states have been considered for each molecule, which further support the experimental spectral assignments for the new species. The optimized structures are presented in Fig. 2.

A linear structure with a closed–shell singlet ground state for OIrF was obtained at both CCSD(T) and B3LYP levels (Table S5, ESI†). The calculated bond length of Ir–F in OIrF is 180.4 pm at the CCSD(T) level, shorter than that in free IrF (186.1 pm) and IrF_2 (184.9 pm).[3] Additionally, this metal–fluorine bond is much shorter than those in OPtF (189.7 pm) and OAuF (188.2 pm) (Fig. S2, ESI†).[11,12] The M–F stretching frequencies

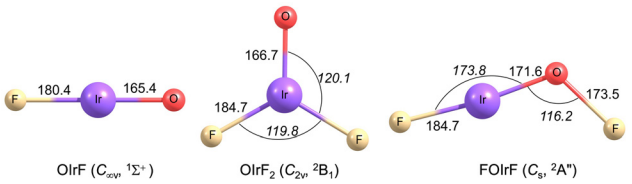

Fig. 2 Optimized structures of OIrF, $OIrF_2$ and FOIrF in their ground states at the CCSD(T)/aug-cc-pVTZ-PP level. Selected bond lengths in pm and angles in deg (in italics) are shown.

in OMF follow the same trend and are confirmed by the experiments (ν(Ir–F) > ν(Au–F) > ν(Pt–F)). Moreover, the CCSD(T) M–O bond distances take large jumps from 165.4 pm for OIrF to 175.1 pm for OPtF to 181.0 pm for OAuF, and the corresponding O–M stretching wavenumbers in OMF decrease continuously from Ir (1053.4 cm^{-1}), Pt (848.3 cm^{-1}) to Au (767.9 cm^{-1}).[11,12] Neither of the O–M vibrational stretches in OMF (M = Ir, Pt and Au) were observed in the experiments (Table S7, ESI†).[11,12] The large differences in M–O bond distances and stretching wavenumbers in OMF (M = Ir, Pt and Au) can be explained by multiple bond character for OIrF, terminal oxyl radical character for OPtF, and biradical character for OAuF.[11,12] The OIrF orbital plots show (Fig. S3, ESI†) one σ bond and two π bonds formed by the O 2p and Ir 5d atomic orbitals, although oxygen has only two unpaired electrons. Similar to the case of the closed–shell OScF molecule,[15] the terminal Ir–O bond in OIrF can be described formally as a triple bond consisting of a σ bond, a π bond and a dative bond where the oxygen 2p lone pair donates electrons into an empty Ir 5d orbital. Consistent with this character, the Ir–O bond distance (165.4 pm) in the OIrF molecule is close to the sum of proposed triple bond radii for iridium and oxygen ([IrO$^+$], 161.5 pm).[21]

At the CCSD(T) level, the hypofluorite FOIrF in C_s symmetry is predicted to have a quartet ground state (^{4}A″), closely followed by 1.2 and 16.5 kJ mol^{-1} less stable ^{4}A′/C_s and ^{2}A″/C_s structures, respectively. However, attempts to optimize a doublet structure for FOIrF failed at the B3LYP level, and the ^{2}A″/C_s state yields one imaginary frequency and the ^{2}A′/C_s state undergoes isomerization to $OIrF_2$ during optimization. While the energy difference favours the ^{4}A″/C_s structure, the vibrational wavenumbers and their $^{16/18}$O isotope shifts for the ^{2}A″/C_s state are in better agreement with our experimental values (Table S4, ESI†). The FIrOF molecule in the ^{2}A″/C_s state has a planar structure in which the FO and IrF moieties adopt a *trans* conformation with respect to the O–Ir bond (∠(Ir–O–F) = 116.2°; ∠(F–Ir–O) = 173.8°) at the CCSD(T) level (Fig. 2), similar to the structure of FOPdF.[12]

$OIrF_2$ is optimized to have a $^2B_1$ ground state with C_{2v} symmetry. The $^4B_2/C_{2v}$ state is 97.4 kJ mol^{-1} higher in energy than the ground state at the CCSD(T) level (Table S1, ESI†). The ∠(F–M–O) angles in OMF_2 (M = Ir, Pt and Au) substantially decrease from Ir to Pt to Au at the CCSD(T) level (Fig. S4, ESI†). The M–O bond distance in $OIrF_2$ (166.7 pm) is slightly longer than that in OIrF (165.4 pm), but is notably shorter than those in $OPtF_2$ (172.8 pm) and $OAuF_2$ (186.1 pm). The significant decrease in the M–O stretching wavenumber from $OIrF_2$ and $OPtF_2$ to $OAuF_2$ is consistent with a significant increase in the M–O bond distance as the M–O bond transitions from a double

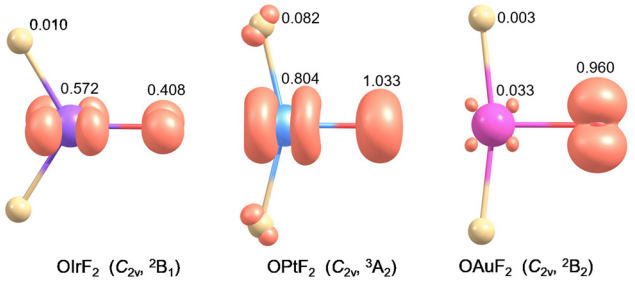

Fig. 3 The spin density (iso-surface = 0.03 electron a.u.$^{-3}$) of $OIrF_2$, $OPtF_2$ and $OAuF_2$ obtained at the B3LYP/aug-cc-pVTZ-PP level.

bond for $OIrF_2$ to a single bond with radical character on the O atom for $OAuF_2$ (Fig. S4 and Table S8, ESI†).[11,12] An analysis of the electronic structures for $OIrF_2$ showed that the unpaired electron of the $^2B_1$ state is found to reside in the Ir–O π^*-antibonding molecular orbital (Fig. S5, ESI†). In contrast to $OPtF_2$ and $OAuF_2$ carrying large spin densities ($\geq$0.96) at the oxygen atom,[11,12] a much lower spin density at the oxygen atom was found in $OIrF_2$, even slightly lower than that at the iridium center (Fig. 3). Comparing the M–F bond distances shows that there is a great increase from $OIrF_2$ (184.6 pm) to $OPtF_2$ (189.2 pm) and $OAuF_2$ (190.0 pm) (Fig. S4, ESI†).

The thermochemical stability of the observed compounds was investigated (Table S9, ESI†). IR-laser ablation generates excited iridium atoms, which are expected to be inserted into the O–F bonds of OF_2 to yield the hypofluorite FOIrF during deposition. The observed main product $OIrF_2$ is likely to have formed from three channels. One is that $OIrF_2$ is produced spontaneously from the reaction of iridium atoms with OF_2, based on sample annealing, during which negligible activation energy is required and the reaction is calculated to be highly exothermic of -929.7 kJ mol^{-1}. Another way of formation is that $OIrF_2$ is formed by an exothermic rearrangement (FOIrF $\rightarrow$ $OIrF_2$ $\Delta E = -389.0$ kJ mol^{-1}) of the initially formed FOIrF. The third way is that OIrF is initially formed from the reaction of iridium atoms and OF radicals, but it reacts rapidly further with F atoms to become $OIrF_2$, which might explain why the OIrF bands are very weak in the experimental observations.

In conclusion, excited Ir atoms were made to react with OF_2 to form the iridium oxyfluoride molecules OIrF, $OIrF_2$ and FOIrF, which have been characterized using matrix-isolation IR spectroscopy and electronic structure calculations. The identification of these compounds was based on the metal–oxygen and metal–fluorine stretches with characteristic $^{16/18}O$ isotopic shifts and support from electronic structure calculations at B3LYP and CCSD(T) levels. The B3LYP calculated molecular orbitals reveal that the linear OIrF molecule in the closed-shell singlet ground state exhibits triple Ir–O bond character. This is in accordance with the shorter bond distance and higher metal–oxygen stretching wavenumber compared with those of OPtF and OAuF. The molecule $OIrF_2$ possesses a planar geometry with C_{2v} symmetry in the $^2B_1$ ground state, for which the unpaired electron is located mainly in the Ir–O π^*-antibonding molecular orbital. A much lower spin-density contribution at the oxygen atom was found in $OIrF_2$, which is in contrast to that in terminal oxyl radical species $OPtF_2$ and $OAuF_2$ with high spin densities at the oxygen atom, along with the sharply increasing M–O bond distance as well as the decreasing FMO bond angles from $OIrF_2$ and $OPtF_2$ to $OAuF_2$.

The authors gratefully thank the Zentraleinrichtung für Datenverarbeitung (ZEDAT) of the Freie Universität Berlin for the allocation of computing resources. The authors thank for the continuous support provided by the ERC Project HighPotOx as well as the CRC 1349 (SFB 1349) Fluorine-Specific Interactions-Project-ID 387284271. Y. L. thanks the China Scholarship Council (PhD Program) for financial support.

Conflicts of interest

There are no conflicts to declare.

Notes and references

1 G. Wang, M. Zhou, J. T. Goettel, G. J. Schrobilgen, J. Su, J. Li, T. Schlöder and S. Riedel, *Nature*, 2014, **514**, 475.
2 (*a*) M. Da Silva Santos, T. Stüker, M. Flach, O. S. Ablyasova, M. Timm, B. von Issendorff, K. Hirsch, V. Zamudio-Bayer, S. Riedel and J. T. Lau, *Angew. Chem., Int. Ed.*, 2022, **61**, e202207688; (*b*) S. Riedel and M. Kaupp, *Coord. Chem. Rev.*, 2009, **253**, 606; (*c*) T. Vogt, A. N. Fitch and J. K. Cockcroft, *Science*, 1994, **263**, 1265; (*d*) E. G. Hope, W. Levason and J. S. Ogden, *J. Chem. Soc., Dalton Trans.*, 1988, 61.
3 Y. Lu, Y. A. Tsegaw, A. Wodyński, L. Li, H. Beckers, M. Kaupp and S. Riedel, *Chem. – Eur. J.*, 2022, **28**, e202104005.
4 (*a*) T. Drews, J. Supel, A. Hagenbach and K. Seppelt, *Inorg. Chem.*, 2006, **45**, 3782; (*b*) A. D. Richardson, K. Hedberg and G. M. Lucier, *Inorg. Chem.*, 2000, **39**, 2787; (*c*) R. T. Paine and L. B. Asprey, *Inorg. Chem.*, 1975, **14**, 1111.
5 O. Ruff and J. Fischer, *Z. Anorg. Allg. Chem.*, 1929, **179**, 161.
6 P. L. Robinson and G. J. Westland, *J. Chem. Soc.*, 1956, 4481.
7 S. Riedel and M. Kaupp, *Angew. Chem., Int. Ed.*, 2006, **45**, 3708.
8 H. Selig, W. A. Sunder, F. A. Disalvo and W. E. Falconer, *J. Fluorine Chem.*, 1978, **11**, 39.
9 M. A. Hepworth and P. L. Robinson, *J. Inorg. Nucl. Chem.*, 1957, **4**, 24.
10 R. C. Burns, T. A. O'Donnell and A. B. Waugh, *J. Fluorine Chem.*, 1978, **12**, 505.
11 L. Li, T. Stüker, S. Kieninger, D. Andrae, T. Schlöder, Y. Gong, L. Andrews, H. Beckers and S. Riedel, *Nat. Commun.*, 2018, **9**, 1267.
12 L. Li, H. Beckers, T. Stüker, T. Lindič, T. Schlöder, D. Andrae and S. Riedel, *Inorg. Chem. Front.*, 2021, **8**, 1215.
13 R. Wei, Z. T. Fang, M. Vasiliu, D. A. Dixon, L. Andrews and Y. Gong, *Inorg. Chem.*, 2019, **58**, 9796.
14 L. Andrews, X. Wang, Y. Gong, T. Schlöder, S. Riedel and M. J. Franger, *Angew. Chem., Int. Ed.*, 2012, **51**, 8235.
15 Y. Gong, L. Andrews and C. W. Bauschlicher, *Chem. – Eur. J.*, 2012, **18**, 12446.
16 Y. Gong, L. Andrews and C. W. Bauschlicher, Jr., *J. Phys. Chem. A*, 2012, **116**, 10115.
17 R. Wei, Q. N. Li, Y. Gong, L. Andrews, Z. Fang, K. S. Thanthiriwatte, M. Vasiliu and D. A. Dixon, *J. Phys. Chem. A*, 2017, **121**, 7603.
18 A. Arkell, R. R. Reinhard and L. P. Larson, *J. Am. Chem. Soc.*, 1965, **87**, 1016.
19 Y. Gong, M. Zhou, M. Kaupp and S. Riedel, *Angew. Chem., Int. Ed.*, 2009, **121**, 8019.
20 A. Citra and L. Andrews, *J. Phys. Chem. A*, 1999, **103**, 4182.
21 P. Pyykkö, S. Riedel and M. Patzschke, *Chem. – Eur. J.*, 2005, **11**, 3511.